

Multi-channel terahertz focused beam generator based on shared-aperture metasurface

Jiu-Sheng Li(李九生) and Yi Chen(陈翊)
Citation: Chin. Phys. B, 2023, 32 (**12**): 124204. DOI: 10.1088/1674-1056/acddd2
Journal homepage: http://cpb.iphy.ac.cn; http://iopscience.iop.org/cpb

What follows is a list of articles you may be interested in

Terahertz shaping technology based on coherent beam combining

Xiao-Ran Zheng(郑晓冉), Dan-Ni Ma(马丹妮), Guang-Tong Jiang(蒋广通), Cun-Lin Zhang(张存林), and Liang-Liang Zhang(张亮亮)
Chin. Phys. B, 2023, 32 (**11**): 114210. DOI: 10.1088/1674-1056/acc2b0

High efficiency of broadband transmissive metasurface terahertz polarization converter

Qiangguo Zhou(周强国), Yang Li(李洋), Yongzhen Li(李永振), Niangjuan Yao(姚娘娟), and Zhiming Huang(黄志明)
Chin. Phys. B, 2023, 32 (**2**): 024201. DOI: 10.1088/1674-1056/ac6db7

Multi-function terahertz wave manipulation utilizing Fourier convolution operation metasurface

Min Zhong(仲敏) and Jiu-Sheng Li(李九生)
Chin. Phys. B, 2022, 31 (**5**): 054207. DOI: 10.1088/1674-1056/ac46c0

Creation of multi-frequency terahertz waves by optimized cascaded difference frequency generation

Zhong-Yang Li(李忠洋), Jia Zhao(赵佳), Sheng Yuan(袁胜), Bin-Zhe Jiao(焦彬哲), Pi-Bin Bing(邴丕彬), Hong-Tao Zhang(张红涛), Zhi-Liang Chen(陈治良), Lian Tan(谭联), and Jian-Quan Yao(姚建铨)
Chin. Phys. B, 2022, 31 (**4**): 044205. DOI: 10.1088/1674-1056/ac29b4

High-sensitive terahertz detection by parametric up-conversion using nanosecond pulsed laser

Yuye Wang(王与烨), Gang Nie(聂港), Changhao Hu(胡常灏), Kai Chen(陈锴), Chao Yan(闫超), Bin Wu(吴斌), Junfeng Zhu(朱军峰), Degang Xu(徐德刚), and Jianquan Yao(姚建铨)
Chin. Phys. B, 2022, 31 (**2**): 024204. DOI: 10.1088/1674-1056/ac2d20

Multi-channel terahertz focused beam generator based on shared-aperture metasurface

Jiu-Sheng Li(李九生)[†] and Yi Chen(陈翊)

Centre for THz Research, China Jiliang University, Hangzhou 310018, *China*

(Received 8 May 2023; revised manuscript received 3 June 2023; accepted manuscript online 13 June 2023)

Most of existing metasurfaces usually have limited channel behavior, which seriouslyhinders their development and application. In this paper, we propose a multi-channel terahertz focused beam generator based on shared-aperture metasurface, and the generator consists of a top square metal strip, a middle layer of silica and a metal bottom plate. By changing the position and size of the shared-aperture array, the designed metasurface can generate any number of multi-channel focusing beams at different predicted positions. In addition, the energy intensity of focusing beams can be controlled. The full-wave simulation results show that the metasurface achieves four-channel vortex focused beam generation with different topological charges, and five-, six-, eight-channel focused beam generation with different energy intensities at a frequency of 1 THz, which are in good agreement with the theoretically calculated predictions. This work can provide a new idea for designing the terahertz multichannel devices.

Keywords: terahertz wave, multi-channel, shared-aperture, focused beam

PACS: 42.50.Tx, 03.65.Vf, 07.05.Tp **DOI:** 10.1088/1674-1056/acddd2

1. Introduction

As a simple and effective method to control electromagnetic waves, coding metasurfaces have attracted extensive attention in recent years.[1–4] By pre-arranging coding elements with different amplitudes and phases based on periodic or aperiodic laws, coding metasurfaces achieve radar cross section (RCS) noise reduction,[5,6] focusing,[7,8] beam splitting,[9,10] vortex,[11,12] etc. For example, in 2020, Han *et al*. designed a metasurface composed of an inner rectangular ring and an outer Jerusalem cross structure combining "C" shaped branch to realize the RCS reduction function.[13] Fu *et al*. proposed a metasurface based on C-shaped symmetric split ring with the central cross-shaped metal structure to generate the suppression of RCS.[14] Shen *et al*. arranged a silicon column structure with graphene electrode to realize an adjustable focusing imaging.[15] Zhou *et al*. also used silicon column structure with external graphene electrode to generate adjustable the position and number of focused beams.[16] In 2021, Gu *et al*. demonstrated a multi-layer metasurface made of anisotropic rectangular patches and cross metal strips to produce splitting vortex beam.[17] Zheng *et al*. used a silicon dielectric square column metasurface based on propagation phase and Pancharatnam–Berry (PB) phase theorem to achieve annular radiation.[18] In 2022, Zhou and Song employed "I" shaped metal structure according to the octagonal spiral sequence to control the vortex beam topological charges by changing the Fermi energy level of graphene.[19] However, the above-mentioned metasurfaces usually have only a single channel and limited functions. A few metasurfaces often require complex calculations to achieve multi-channel functionality, and most of these metasurfaces mainly operate in an infrared or microwave frequency band.[20–22] And composite multichannel and multifunctional focused beam generators based on reflective metasurface in a terahertz region are rarely reported. In this article, we propose a coding metasurface with shared-aperture nesting and parallel connection, which can generate any number of focused beams at any position. By changing the size of the shared aperture array, the designed structure can also control the energy intensity of the focused beam.

Here, the proposed multichannel terahertz focused beam generator consists of a square metal bar layer and a metallic bottom plane layer, between which a silica substrate is sandwiched. The simulation results shows that complete 2π phase coverage can be obtained in a frequency ranging from 0.8 THz to 1.2 THz by independently rotating the metallic strip structures for normally incident RCP (right circularly polarized) wave. And then, we design the vortex focus metasurface with a focus length of $F = 1000$ μm for the topological charges of $l = \pm 1$ and $l = \pm 2$. Furthermore, we also realize four-channel focused beam and vortex focused beam generation with different topological charges. Moreover, by replacing part of the array group with a shared-aperture array method, the designed metasurface generates five-, six-, and eight-channel focused beams with different energy intensities. The numerical simulation results are in good agreement with the theoretical predictions. Our structure provides a new method of designing terahertz multichannel mesurface-based devices, which can greatly extend the functions and the application scope of metasurface. This structure also provides a new method of manipulating the terahertz wave communication and detection.

[†]Corresponding author. E-mail: lijsh2008@126.com

© 2023 Chinese Physical Society and IOP Publishing Ltd

2. Structure design

Figure 1 shows a schematic diagram of the multi-channel terahertz focused beam generator based on a shared-aperture principle. When RCP wave is incident along the $-z$-axis direction, the matasurface produces multiple channels reflected LCP focusing beams. The unit-cell is composed of a top square metal strip, an intermediate dielectric layer, and a bottom metal plate, as shown in Figs. 1(b) and 1(c). The dielectric substrate layer is of silicon dioxide with a dielectric constant of 3.9 and loss angle of 0.0004.[23] The metallic parts in top layer and bottom layers are of gold with a conductivity of 4.6×10^7 S/m and a thickness of 1 μm. By using the commercial software CST Microwave Studio, we simulate and optimize the electromagnetic transmission amplitude and phase response of the unit cell. The optimized geometric parameters of our proposed unit-cell are as follows: $a = 10$ μm, $b = 90$ μm (Here, the parameter scanning results are displayed in Figs. 2(a) and 2(b)), and the period of the unit cell $P = 100$ μm. In addition, the thickness of the silicon dioxide is 40 μm.[24] In order to meet the gradient phase, eight kinds of coding elements are designed and illustrated in Table 1, where φ is the gradient phase of the corresponding unit cell, and α is the rotation angle of the unit cell along the y axis. The corresponding reflection coefficient (CRC) and phases under RCP wave incidence are shown in Figs. 2(c) and 2(d). From the figure, one can see that the reflection coefficients of the eight kinds of unit cells are larger than 0.9 THz at 1 THz, and the phase spectra are parallel to each other with a phase difference of 45°.

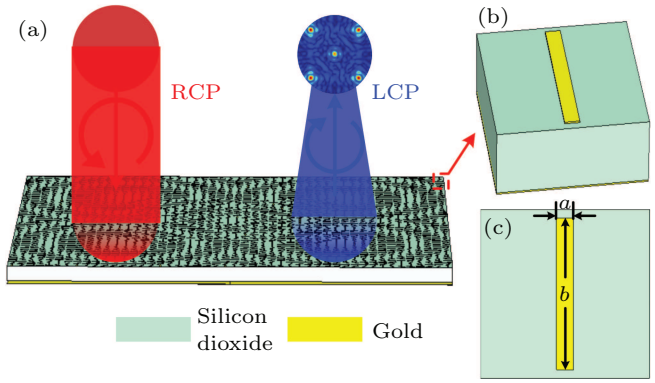


Fig. 1. (a) Function sketch, (b) three-dimensional view of unit cell, and (c) top view of unit cell, for proposed multi-channel terahertz focused beam generator.

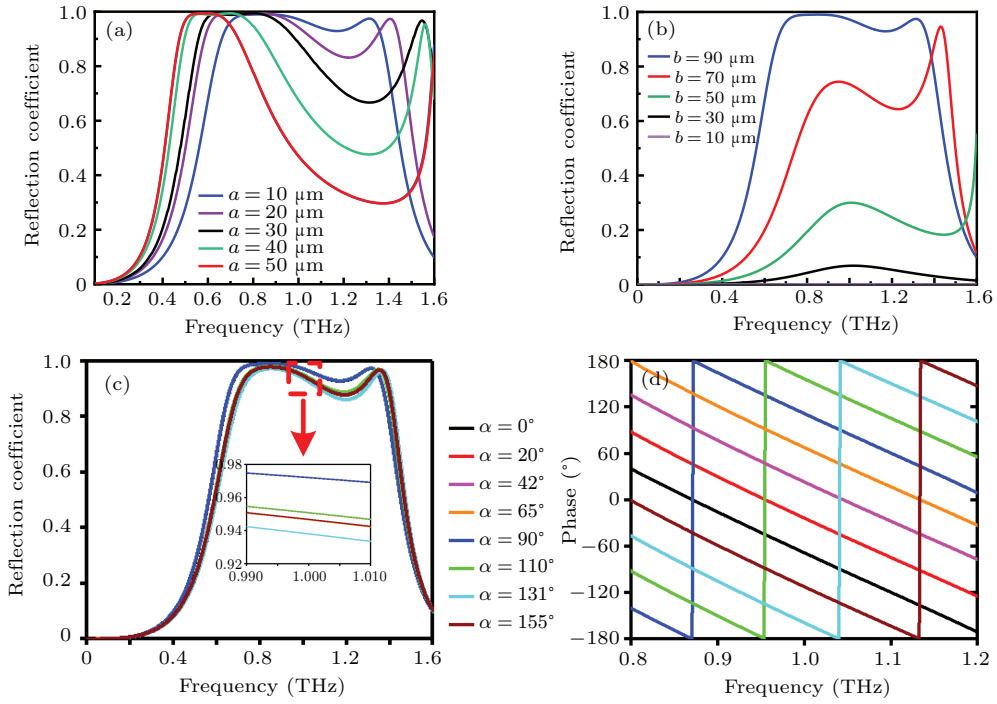


Fig. 2. Reflection coefficients versus frequency for different values of (a) reflection coefficient a, (b) phase b, (c) reflection coefficient α, and (d) phase versus frequency.

Table 1. Top-view, gradient phase, rotation angle, corresponding reflection coefficients, and phase of 8 kinds of coding elements at frequency of 1 THz.

Unit cell	1	2	3	4	5	6	7	8
Top view								
φ	0	$\pi/4$	$\pi/2$	$3\pi/4$	π	$5\pi/4$	$3\pi/2$	$7\pi/4$
α	0°	20°	42°	65°	90°	110°	131°	155°
CRC	0.972	0.951	0.938	0.946	0.972	0.951	0.938	0.947
Phase	−69°	−24°	23°	67°	111°	156°	−159°	−113°

3. Simulation results and analysis

To generate a focused beam, the phase $\varphi_{\mathrm{A}}(x, y)$ of the coding metasurface need to satisfy the following relation:

$$\varphi_{\mathrm{A}}(x,y) = \frac{2\pi}{\lambda}\left(\sqrt{F^2+x^2+y^2}-F^2\right), \tag{1}$$

where x and y represent the horizontal coordinate and vertical coordinate of the unit cell, λ is the working wavelength, F denotes the focal length. Herein, the focal length of the focused beam is set to $F = 1000$ μm, and the structure consists of 48×48 coding elements. Figure 3(a) gives the phase distribution of the designed metasurface structure.

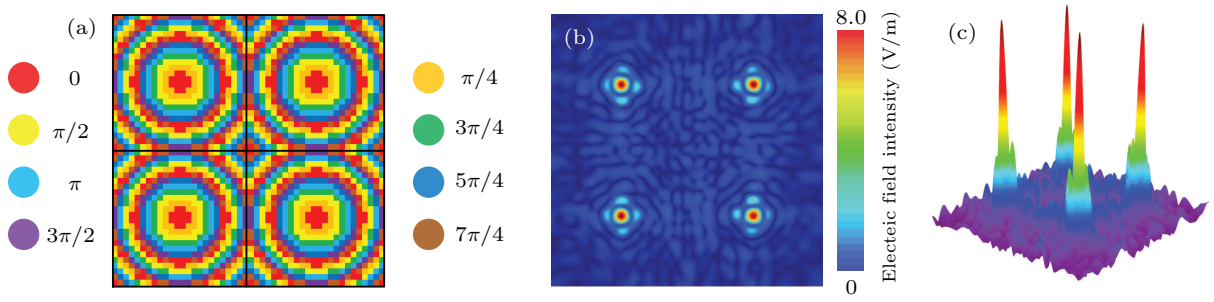


Fig. 3. (a) Phase distribution, (b) top view, (c) 3D view of four-channel focused beam electric field.

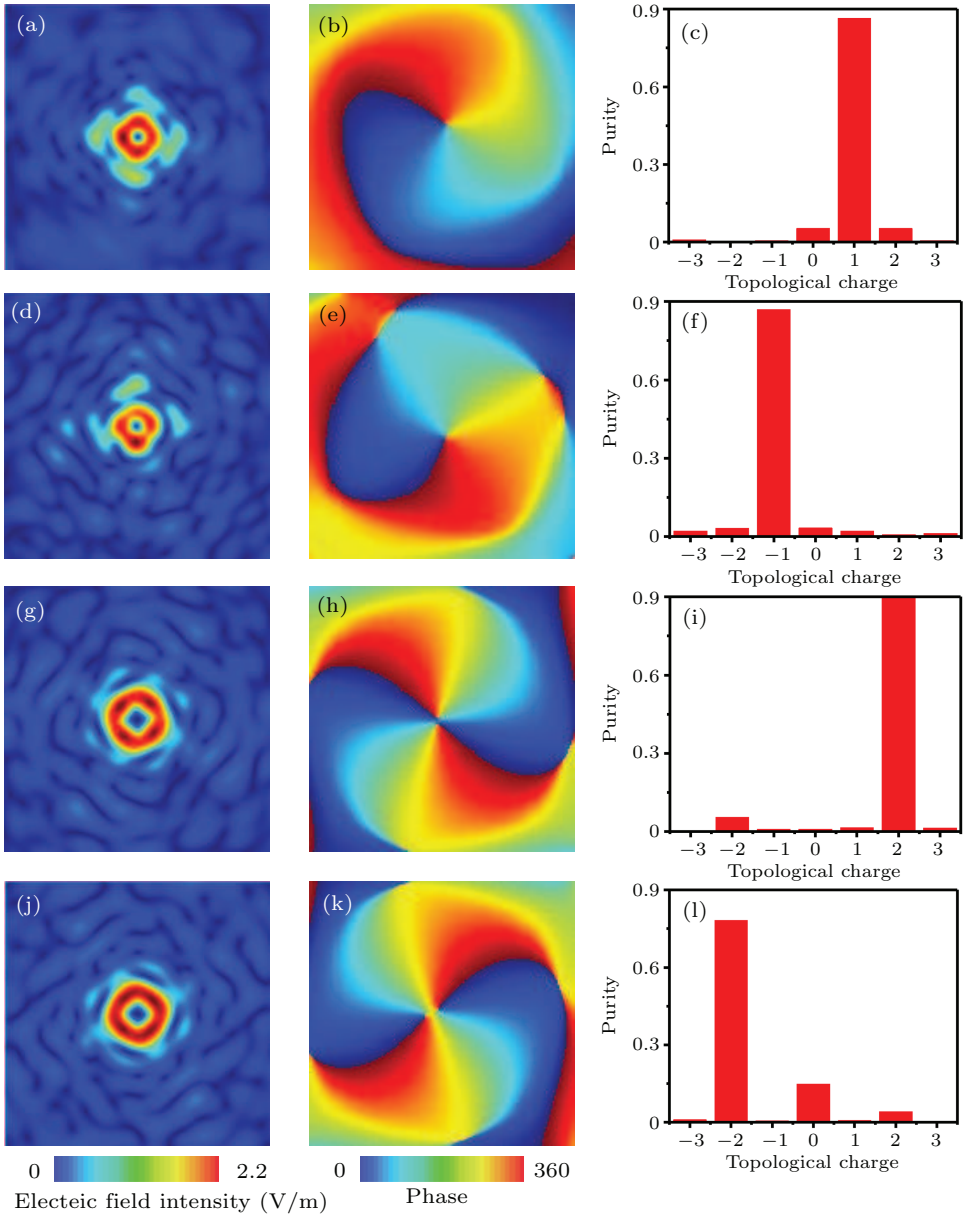


Fig. 4. Electric field strength, phase and mode purity of the vortex focused beams with different topological charges at 1 THz, (a)–(c) $l = 1$, (d)–(f) $l = -1$, (g)–(i) $l = 2$, (j)–(l) $l = -2$.

The electric field distribution in the *xoy* plane at the focal point and three-dimensional (3D) electric field distribution are displayed in Figs. 3(b) and 3(c), respectively. The scales of the simulated multi-channel focused beam field patterns are all 4800 μm×4800 μm. Under the RCP wave normal incidence, the designed structure generates a four-channel focused beam, as illustrated in Fig. 3. One can see that the reflected four-focused beams have the same electric field intensity. The electric field efficiency of the focused beam η can be given by

$$\eta = \frac{\int E_{\mathrm{RL}}^2 \,\mathrm{d}s}{\int E_{\mathrm{OR}}^2 \,\mathrm{d}s} \times 100\%, \tag{2}$$

where E_{OR} is the incident RCP electric field and E_{RL} is the reflected LCP wave electric field. According to Eq. (2), we can obtain that the electric field efficiency of four-channel focused beam is 33.0%.

Furthermore, we design a four-channel vortex focusing metasurface based on parallel array by combining the convolution theorem. In order to realize the vortex focusing function, the distribution law of the phase $\varphi_{\mathrm{B}}(x, y)$ can be expressed as

$$\varphi_{\mathrm{B}}(x,y) = l \cdot \tan^{-1}\left(\frac{y}{x}\right) + \frac{2\pi}{\lambda}\left(\sqrt{F^2+x^2+y^2} - F^2\right), \tag{3}$$

where l is the topological charges of the vortex beam. Figure 4 illustrates the electric field, phase and mode purity of vortex focusing beam for the topological charges of $l = \pm 1$ and ± 2 with a focal length of $F = 800$ μm at frequency of 1 THz. From the figure, one can see that the phase of the vortex focusing beam rotates counterclockwise as the topological charges are positive. Likewise, when the topological charges are negative value, the phase of the vortex focusing beam rotates clockwise. Furthermore, the mode purities of the vortex focusing beam with topological charges $l = \pm 1$ and ± 2 are 87.46%, 87.01%, 86.47%, and 78.31%, respectively. It is worth noting that the electric field diagram of the vortex focused beam is a ring with a dark spot in the center. The more the topological charges, the bigger the dark spot is. It is because the OAM vortex beam has a phase singularity, which causes the center field of the vortex beam to approach to 0. Figure 5(a) shows four vortex focusing metasurface arrays. The electric field and phase at the focal length are displayed in Fig. 5(b). Obviously, the topological charges of vortex focusing beam in the upper-left channel, upper-right channel, lower-left channel and lower-right channel are $l = 1$, -1, 2, and -2, respectively. And then, the corresponding electric field intensities are 3.1 V/m, 3.0 V/m, 2.7 V/m, and 2.6 V/m, respectively. The electric field efficiency of four-channel focused vortex beam is 55.5%. Their corresponding phases are shown in Figs. 5(c)–5(f). In addition, from Fig. 5(b), one can see that the vortex focusing beam has an annular profile. The diameter of the vortex focusing beam with topological charges of $l = \pm 1$ is significantly smaller than that of the vortex focusing beam with topological charges of $l = \pm 2$. It also verifies that the size of the vortex focusing beam depends on the topological charges.

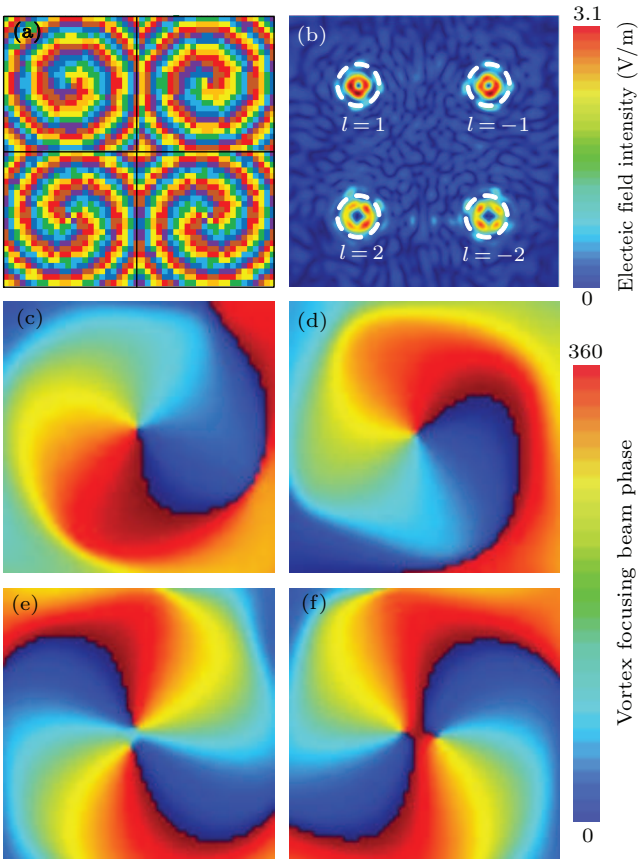


Fig. 5. (a) Phase distribution of four-channel metasurface, (b) electric field strength of four-channel vortex focused beam, vortex focused beam phases with different topological charges of $l = 1$ (c), -1 (d), 2 (e), and -2 (f).

To expand the channel number of the focused beam, a multi-channel terahertz focusing beam metasurface is proposed by combining the shared-aperture interlace cascade and array parallel arrangement. The shared-aperture metasurface consists of multiple interlaced sub-arrays, which share the same aperture of the metasurface. Each sub-array carries a geometric phase profile, which can stimulate different spatial channels for different functions. In order to obtain favorable performance, it is desirable to arrange sub-arrays regularly or randomly in an interlaced manner, rather than aggregate the unit cells of sub-arrays in local areas. Typically, in order to maintain relatively equal energy in each channel, different sub-arrays need to contain approximately the same number of unit cells. Figure 6 provides a schematic diagram of the principle of multi-channel functional multiplexing metasurface combining array parallel and shared-aperture. Figure 6(b) displays the middlepart phase distribution of the four-channel focused parallel array (see Fig. 6(a)), and Fig. 6(c) shows the phase distribution of the focusing beam with focal length $F = 1000\mu$m. The two sub-arrays are staggered according to the following

relation:

$$\begin{cases} \varphi(i,j) = \varphi_1(i,j), & \text{Mod}(|i-j|, N) = 0, \\ \varphi(i,j) = \varphi_2(i,j), & \text{Mod}(|i-j|, N) = 1, \\ & \cdots \\ \varphi(i,j) = \varphi_N(i,j), & \text{Mod}(|i-j|, N) = N-1, \end{cases} \tag{4}$$

where N represents the number of sub-arrays which are used to constructe the main array, φ^1–φ^N denote the phase distribution of the 1st to Nth sub-arrays, i and j are the position of the corresponding unit cell along x axis and y axis in the array, respectively. Figure 6(d) gives the phase distribution between the main array and the sub-array for $N = 2$. Here, the sub-array 0 denotes the array in Fig. 6(b), and the sub-array 1 is the array in Fig. 6(c). The two-dimensional (2D) electric field intensity of the five-channel focused beam generated by the shared-aperture parallel array is shown in Fig. 6(g). Figure 6(h) displays 3D electric field distribution of the five-channel focusing beam. As can be seen from the figure, the electric field intensity of the focused beam in upper left, upper right, lower left and lower right channel are 4.4 V/m, 4.2 V/m, 4.3 V/m, and 4.4 V/m respectively. In addition, the electric field intensity of the focused beam in the middle channel equals 3.4 V/m. The electric field efficiency of five-channel focused beam is 43.4%.

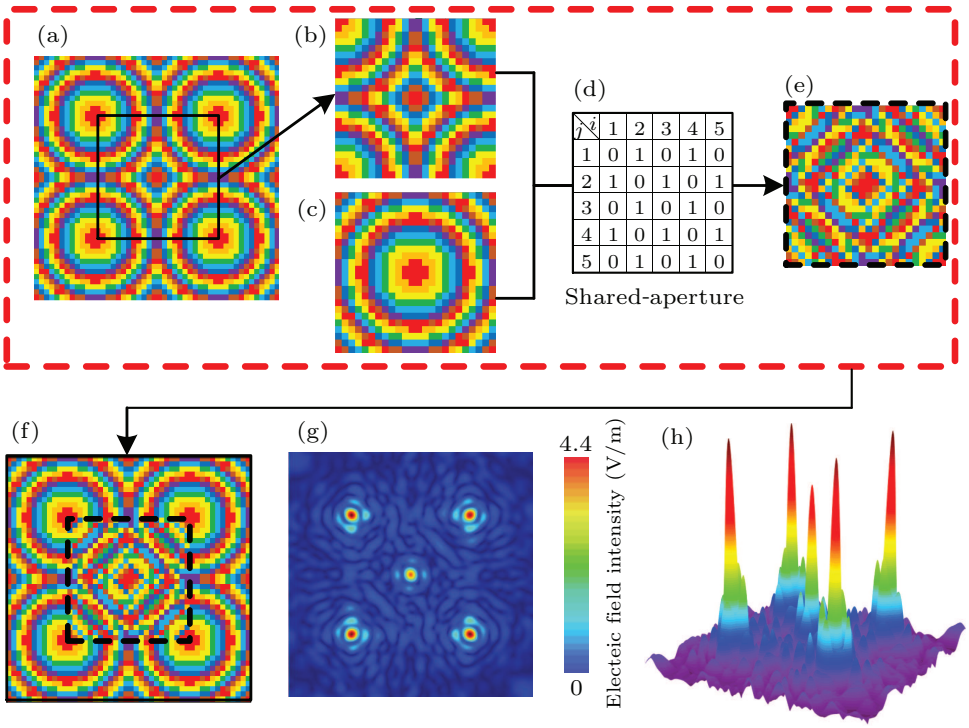


Fig. 6. (a) Phase distribution of four-channel focusing metasurface, (b) middle-part phase distribution of the four-channel focusing metasurface (black dash-line), (c) single-focusing metasurface, (d) dual-channel shared-aperture array pattern, (e) middle-part phase distribution of the five-channel focusing metasurface, (f) phase distribution of five-channel focusing metasurface, (g) 2D and (h) 3D electric field intensities of the five-channel focusing beam.

Figure 7(f) illustrates the phase configuration diagram of the six-channel focusing beam metasurface, in which the phase configurations of the middle-up part and middle-low part are shown in Fig. 7(e). In fact, the middle-part phase configuration can be obtained by staggered cascade arrangement of the metasurface arrays (*i.e.* Figs. 7(b) and 7(c)) based on shared-aperture. The electric field distribution of the six-channel focusing beam with a focal length of 820 μm is given in Fig. 7(g). Figure 7(h) shows 3D electric field distribution of the focused beam. One can see that the electric field intensity of the focused beam in upper left, upper-right channel, lower-left channel, and lower-right channel are 3.7 V/m, 3.7 V/m, 3.6 V/m and 3.7 V/m, respectively. In addition, the electric field intensity of the middle and upper channels are 2.84 V/m and 2.83 V/m, respectively. The electric field efficiency of six-channel focused beam is 24.2%.

Furthermore, by replacing the intermediate array in Fig. 6 with a four-channel focusing parallel array, we obtain an eight-channel focusing beam. Figure 8(f) shows the phase diagram of the eight-channel focusing beam metasurface. The phase distribution of the middle array part is displayed in Fig. 8(e). We can find that the array based on 24×24 unit cells is generated by the middle part of the four-channel focusing array (see Fig. 8(b)) and the four-channel focusing parallel array (see Fig. 8(c)) by using shared-aperture principle. The electric field distribution of the eight-channel focusing beam with a focal length of 760 μm is displayed in Figs. 8(g) and 8(h), which is in good agreement with the theoretical result. As can be seen from the figure, the focusing beam electric field intensity of the upper-left channel, upper-right channel, lower-left channel, and lower-right channel of the outer ring are 6.1 V/m, 5.8 V/m, 5.8 V/m, and 5.9 V/m, respectively. Furthermore, the

focused beam electric field intensity of the upper-left channel, upper-right channel, lower-left channel, and lower-right channel of the inner circle are 1.9 V/m, 1.8 V/m, 1.9 V/m, and 1.9 V/m, respectively. The electric field efficiency of eight-channel focused beam is 62.9%. The proposed metasurface arrangement method based on shared-aperture can not only generate any number of focused beams at any position, but also control the energy intensity of focused beams.

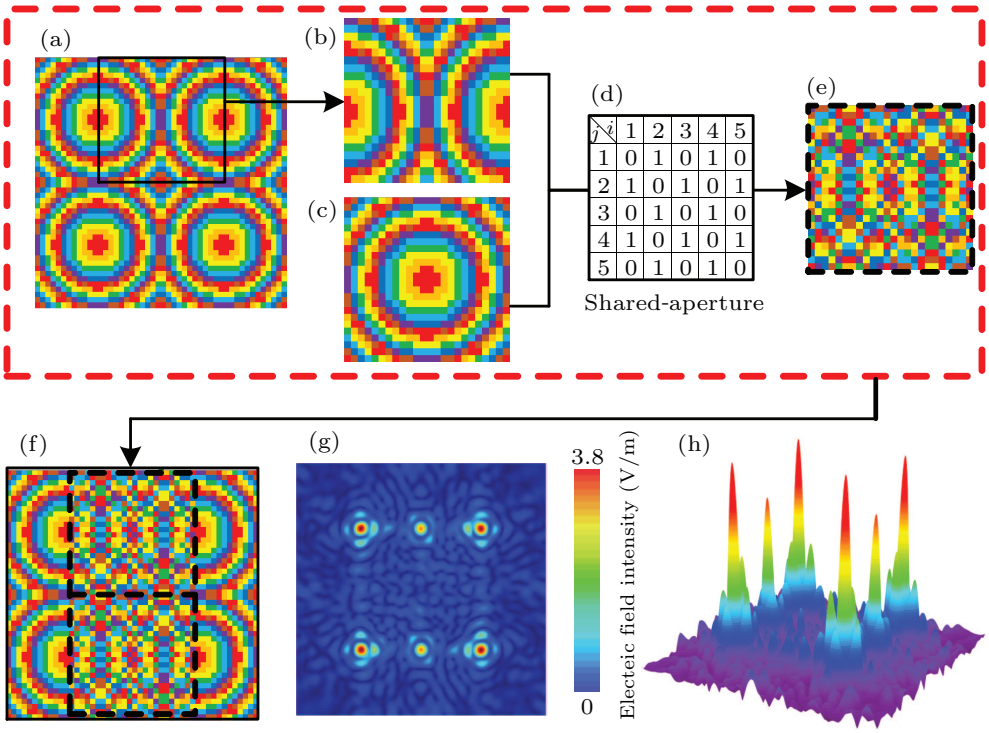


Fig. 7. (a) Phase distribution of four-channel focusing metasurface, (b) middle-up-part phase distribution of the four-channel focusing metasurface (black dash-line), (c) single-channel focusing metasurface, (d) dual-channel shared-aperture array pattern, (e) middle-part phase distribution of six-channel focusing metasurface, (f) phase distribution of six-channel focusing metasurface, (g) 2D and (h) 3D electric field intensities of six-channel focused beam.

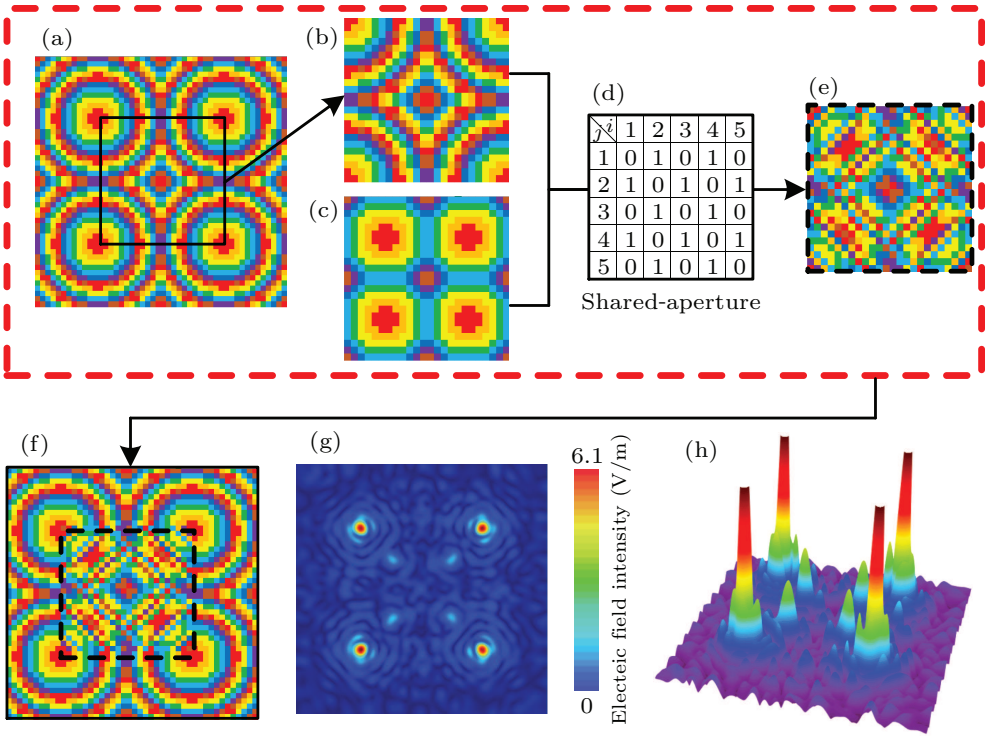


Fig. 8. (a) Phase distribution of four-channel focusing metasurface, (b) middle-part phase distribution of the four-channel focusing metasurface (black dash-line), (c) four-channel focusing metasurface (2400 μm×2400 μm), (d) dual-channel shared-aperture array pattern, (e) middle-part phase distribution of eight-channel focusing metasurface, (f) phase distribution of eight-channel focusing metasurface, (g) 2D and (h) 3D electric field intensity planes of eight-channel focused beam.

4. Conclusions

In this work, a metasurface based on shared-aperture is proposed to generate multi-channel terahertz vortex focused beam and multi-channel terahertz non-vortex focused beam. The patterned unit cell structure consists of a top square metal strip layer, a middle silicon dioxide layer, and a bottom metallic plate. Full-wave simulation results and theoretical calculation results show that the metasurface generates multi-channel focused LCP wave at 1 THz for a normally incident RCP wave. Through parallel array arrangement, the proposed metasurface achieves four-channel vortex focused beam generation and four-channel vortex focused beam generation with different topological charges $l = \pm 1$, and $l = \pm 2$. Further, by replacing part of the area in the parallel array group with a shared-aperture array, the proposed metasurface realizes five-, six- and eight-channel focused beam generator with different energy intensities. The shared-aperture metasurface paves the way for designing the multi-channel terahertz devices.

Acknowledgements

Project supported by the National Natural Science Foundation of China (Grant No. 62271460) and the Zhejiang Key Research and Development Project, China (Grant Nos. 2021C03153 and 2022C03166).

References

[1] Wei J, Qi Y, Zhang B, Ding J, Liu W and Wang X 2022 *Opt. Commun.* **502** 127425
[2] Li H, Li Y, Chen G, Dong S, Shen J, Gong C, Wang, Wang H and Cui T 2022 *Adv. Mater. Technol.* **7** 2101067
[3] Fu T, Wang D, Yang Z, Deng Z and Liu W 2021 *Opt. Express* **29** 26983
[4] Deng Z, Shi T, Krasnok A, Li X and Alù A 2022 *Nat. Commun.* **13** 8
[5] Zhao Z, Zhang Y, Wu T, Chen S, Li W and Guan J 2021 *Materials* **14** 2787
[6] He X, Qi C and Wong A 2022 *J. Phys. D: Appl. Phys.* **55** 355104
[7] Ya M, Sun Z, Wu B, Cheng P and Xu B 2020 *Front. Phys.* **8** 46
[8] Lee W, Jo S, Lee K, Park H, Yang J, Hong H, Park C, Hong S and Lee H 2021 *Sci. Rep.* **11** 12671
[9] Xue C, Zou H, Su M, Tang L, Wang C, Chen S, Su C and Li Y 2021 *Nanomaterials* **11** 1137
[10] Lv B, Ouyang C, Zhang H, Xu Q, Li Y, Zhang X, Tian Z, Gu J, Liu L, Han J and Zhang W 2020 *IEEE Photon. J.* **12** 1
[11] Kim M and Kim S 2021 *Optik* **247** 167856
[12] Dai Q, Li Z, Deng L, Zhou N, Deng J, Tao J and Zheng G 2020 *Opt. Lett.* **45** 3773
[13] Han X, Xu H, Chang Y, Lin M, Zhang W, Wu X and Wei X 2020 *IEEE Access* **8** 162313
[14] Fu C, Han L, Liu C, Lu X and Sun Z 2020 *J. Phys. D: Appl. Phys.* **53** 445107
[15] Shen Z, Zhou S, Li X, Ge S, Chen P, Hu W and Lu Y 2020 *Adv. Photon.* **2** 036003
[16] Zhou S, Shan Z, Li X, Ge S, Lu Y and Hu W 2020 *Opt. Lett.* **45** 4324
[17] Gu C, Yang R and Li Y 2021 *Opt. Express* **29** 20121
[18] Zheng C, Li J, Wang G, Liu J, Li J, Yue Z, Zhao H, Hao X, Zhang Y, Zhang Y and Yao J 2021 *Nanophotonics* **10** 2959
[19] Zhou Z and Song Z 2022 *Opt Laser Technol.* **153** 108278
[20] Maguid E, Yulevich I, Veksler D, Kleiner V, Brongersma M and Hasman E 2016 *Science* **352** 1202
[21] Jin J, Pu M, Wang Y, Li X, Ma X, Luo J, Zhao Z, Gao P and Luo X 2017 *Advanced Materials Technologies* **2** 1600201
[22] Zhao H, Quan B, Wang X, Gu C, Li J and Zhang Y 2018 *ACS Photon.* **5** 1726
[23] Yi Z, Chen J, Cen C, Chen X, Zhou Z, Tang Y, Ye X, Xiao S, Luo W and Wu P 2019 *Micromachines* **10** 194
[24] Shen H, Liu F, Liu C, Zeng D, Guo B, Wei Z, Wang F, Tan C, Huang X and Meng H 2020 *Nanomaterials* **10** 1410